TECHNICAL TRANSACTIONS | **CZASOPISMO TECHNICZNE**
ELECTRICAL ENGINEERING | ELEKTROTECHNIKA
2-E/2016

DOI: 10.4467/2353737XCT.16.245.6044

JANUSZ GOŁDASZ, BOGDAN SAPIŃSKI*

NUMERICAL STUDY OF A TWO-WAY MR MOUNT IN SQUEEZE-MODE

OBLICZENIOWE STUDIUM TŁUMIKA Z CIECZĄ MR W TRYBIE ŚCISKANIA

A b s t r a c t

In the paper, the authors present the results of a numerical study of a magnetorheological (MR) damper prototype operating in the so-called squeeze mode. The analyzed prototype allows achieving a symmetrical response in both directions of piston motion. The authors show the results of magnetostatic analyses of the electro-magnetic circuit of the device and lumped parameter model using calculations of the control circuit and the damping force output.

Keywords: magnetorheological damper, squeeze-mode, lumped parameter model

S t r e s z c z e n i e

W artykule przedstawiono wyniki obliczeń prototypowej konstrukcji tłumika z cieczą MR działającej w trybie ściskania. Analizowany prototyp pozwala uzyskać identyczny zakres sił tłumienia w obu kierunkach ruchu. Autorzy prezentują osiągi tłumika oszacowane na podstawie obliczeń polowych oraz obliczeń z wykorzystaniem modelu o parametrach skupionych.

Słowa kluczowe: tłumik magnetoreologiczny, tryb ściskania, model o parametrach skupionych

* D.Sc. Ph.D. Eng. Janusz Gołdasz, Department of Automatic Control and Information Technology, Faculty of Electrical and Computer Engineering, Cracow Uniwersity of Technology.

** Prof. D.Sc. Ph.D. Eng. Bogdan Sapiński, Department of Process Control, Faculty of Mechanical Engineering and Robotics, AGH University of Science and Technology.

1. Introduction

A magnetorheological fluid (MRF) is a representative of smart materials that links two separate categories: solids and liquids. The so-called MR effect, discovered by Rabinov [1], is manifested by changes in the material's apparent viscosity when exposed to a magnetic field of sufficient strength. This property has made it attractive for use in the automotive industry, for example. By considering the manner in which the material has been utilized in particular devices, MR devices can be categorized as those operating in four categories: flow mode, shear mode, squeeze mode and gradient pinch mode [2–4]. So far, only the shear mode and flow mode have been commercialized through rotary brakes, automotive suspension dampers and powertrain mounts [5–7]. For comparison, the squeeze-mode offers several benefits over the other operating modes; namely, the ability to build high damping forces across a relatively small displacement span, large compressive stresses, etc. [8, 9]. Typical squeeze-mode devices feature a relatively small volume of MRF contained between two planar surfaces [10–12]. The distance between the surfaces is allowed to vary according to the prescribed displacement or force input. The squeeze-mode devices are outstanding in the sense that they feature a flow channel of time-varying height. As the surface-to-surface distance decreases, the fluid is squeezed out of the working volume. In the presence of magnetic flux, the yield stress of the MRF, which is contained in the working volume, increases along with its resistance-to-flow. With such an arrangement, the actuators are capable of producing compressive forces that are larger by an order of magnitude or more than in extension [13, 14]. However, some vibration control applications may require equal forces in either direction of the piston motion. So far, little work has been done with squeeze-mode actuators that produce symmetric forces in compression as well as extension [9, 15]. For example, the actuator of Gong [15] was a single-coil, dual cavity device capable of producing forces up to 6 kN over a 1.2 mm travel range. Next, in a feasibility study, Stanway *et al*. [16] showed the ability to control the transmissibility of a two-way single and coil squeeze-mode vibration isolator with a simple on-off strategy.

In this paper, the authors briefly examine the concept of a two-way MR actuator operating in a squeeze-mode. In section 2, the authors present the actuator's geometry and key details, and then in section 3, they reveal the results of a magnetostatic study in order to assess the performance range of the device. In section 4, the analysis is followed by a numerical evaluation of the performance of the prototype subjected to sinusoidal displacement inputs for a prescribed range of excitation inputs, incl. electrical characteristics of the coil circuit and damping force output. Finally, section 5 contains the conclusions and a summary.

2. Damper

The squeeze-mode damper assembly concept is revealed in Fig. 1. Specifically, Fig. 1a and Fig. 1b show the device in a cross-section view. As illustrated, the motion of the rod (2) drives the piston (1) displacement. The distance between the lower surface of the piston (1) and the lower surface of the core (3) constitutes the lower working gap. In a similar fashion, the distance between the lower surface of the piston (1) and the opposed

surface of the core 4 constitutes the upper working gap. Both working gap volumes are filled with MRF. Upon the piston displacement, the fluid may flow through the holes (3) into the opposite gap volume. In the magnetostatic analysis performed by the authors, the thru-holes were replaced by a thinner cross-section area of the piston at the location of the holes. The assembly incorporates two cores (4, 5) located on either side of the piston. In this particular configuration, the coils (6, 7) are connected in series. They are wound in opposite directions. The current in the coil induces a magnetic field of the strength H in each core assembly. Specifically, the magnetic flux that is generated by the current in the control coil (6) travels through the core (4), into the upper gap volume and into the piston (1), the cylinder (8) and the cap (9), then to enter the core again. Similarly, the flux induced by the current in the coil (5) travels through the core (3), the lower gap and into the piston. Next, it enters the outer cylinder and returns to the core (3) through the lower cap.

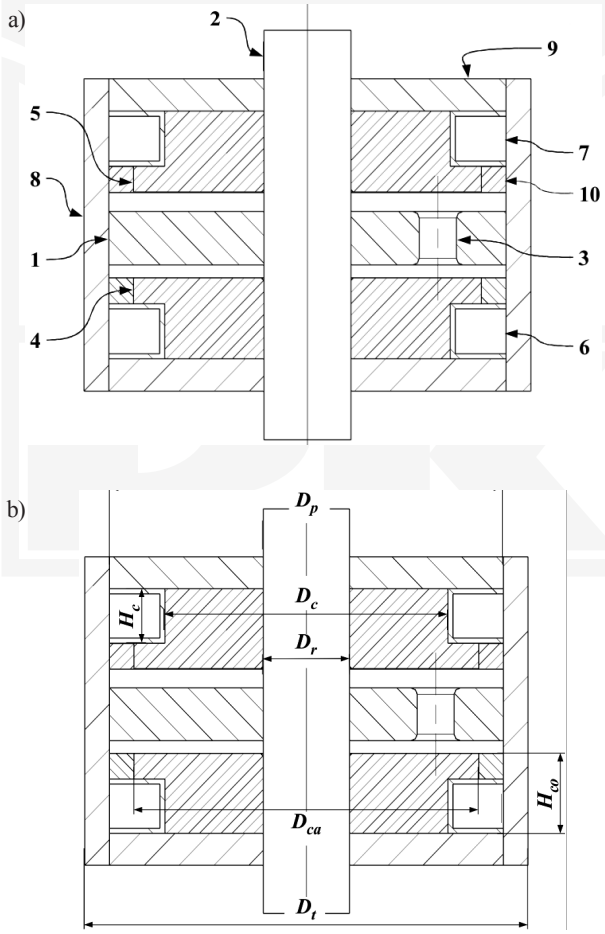

Fig. 1. Squeeze-mode damper cross-section: 1 – piston, 2 – rod, 3 – thru-hole, 4, 5 – cores, 6, 7 – coils, 8 – cylinder, 9 – cap, 10 – ring

The presence of the flux in each gap alters the MRF's resistance-to-flow by modifying its yield stress. The non-magnetic rings (10) surrounding each core assembly eliminate the magnetic flux leakage directly into the core. Fig. 1 does not reveal several engineering details that were omitted for clarity; namely, coil wiring, electrical terminals, sealing systems, and a volume compensating chamber.

The piston is free to move within the cavity, as shown in Fig. 2, across the gap height h. The total permitted travel for the piston is $2(h\text{-}h_{min})$, where h_{min} denotes the minimum gap height in upward (downward) motion to the percent of piston-core contact. All other relevant damper dimensions are highlighted in Table 1. For the purpose of the presented analysis, the authors

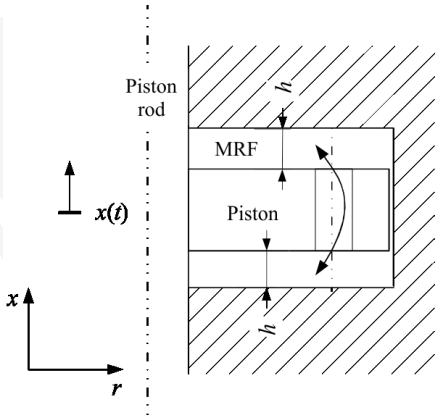

Fig. 2. Working cavity layout, $x(t)$ – piston displacement, h – free gap, MRF – MR fluid

Table 1

Damper dimensions

Parameter	Value, [mm]
Piston diameter, D_p	64
Outer diameter (cylinder), D_t	73
Rod outside diameter, D_r	12
Upper (lower) core surface diameter, D_c	56
Coil window height, H_c	11
Coil window width, W_c	8.5
Core height, H_{co}	19.5
Working gap height, h	2.5
Minimum gap, h_{min}	0.5

assumed the MRF to be of the 26% Fe vol. type. The fluid density was $\rho = 2.6$ g/cm^3, and the base viscosity $\mu = 50$ cP. Accordingly, silicon alloy (SiFe) steel properties were assumed for all the ferromagnetic components of the magnetic circuit (cores, piston, cylinder and cap). The magnetization characteristics of the materials are shown in Fig. 3a, and the yield stress variation with flux density in Fig. 3b. Each coil window incorporates 90 turns of the 0.6 mm copper wire. Effectively, the coils' total resistance was estimated to be 1.94 Ω (at 25°C). Excluding insulation, the effective area of each coil window was 72 mm^2. The piston rod should be made of a non-magnetic material to prevent a magnetic short circuit and flux leakage directly into the piston.

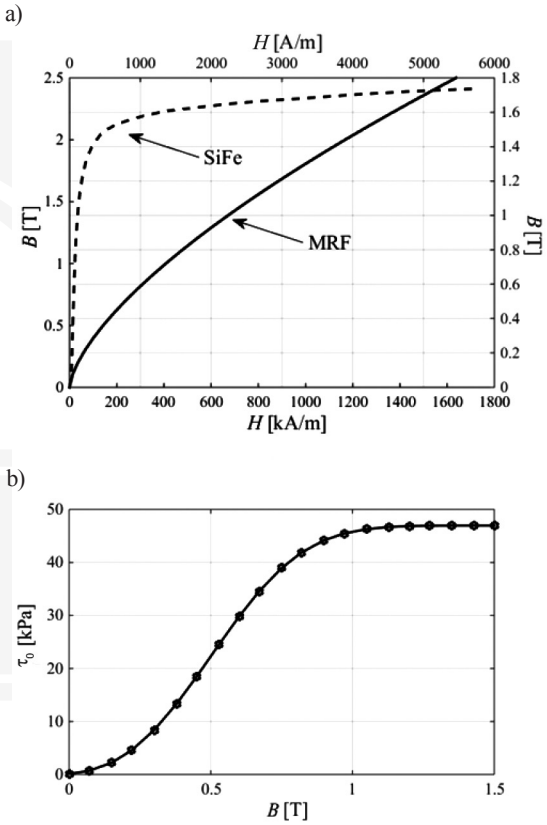

Fig. 3. Material properties: a) magnetization B–H characteristics: silicon (SiFe) steel and MRF, b) MRF's yield stress vs. flux density, τ_0–B [21]

3. Magnetostatic analysis

In order to assess the steady-state performance of the magnetic circuit of the actuator, a 2D-axisymmetric model was developed and analyzed using the software tool FEMM 4.2 [17]. 3D features (thru-holes in the piston assembly) were accounted for in the analysis

by decreasing the piston cross-section area at the location of the holes – see Fig. 4. The purpose of this exercise, at this point, was to evaluate the magnetic flux change and identify problematic areas in the actuator. The analysis was performed within the coil current range from 0.25 A to 5 A. The results that are shown in Figs. 5a and 5b reveal the usable current range is rather limited to 4 A due to magnetic saturation at the mid-stroke position of the damper. The current range is position-dependent due to magnetic saturation. For comparison, at the minimum working gap condition on either side of the piston, it reduces to 3 A. The identified bottleneck areas were due to the thru-holes in the piston assembly, outer cylinder wall, and at either end of the actuator. At this condition, the averaged flux density in each working gap at the mid-stroke position of the piston approaches 0.5 T (and 0.6 T at a minimum working gap condition – piston-to-core distance is 0.5 mm). In addition, based on observations of the results in Figs. 5a and 5b, it seems that the active radius of the actuator extends to approximately 22 mm; the active surface area directly contributes to the damping force output of the actuator. Specifically, Fig. 5a shows the uniform distribution of flux density in the working gap region well within the area defined by the active radius,

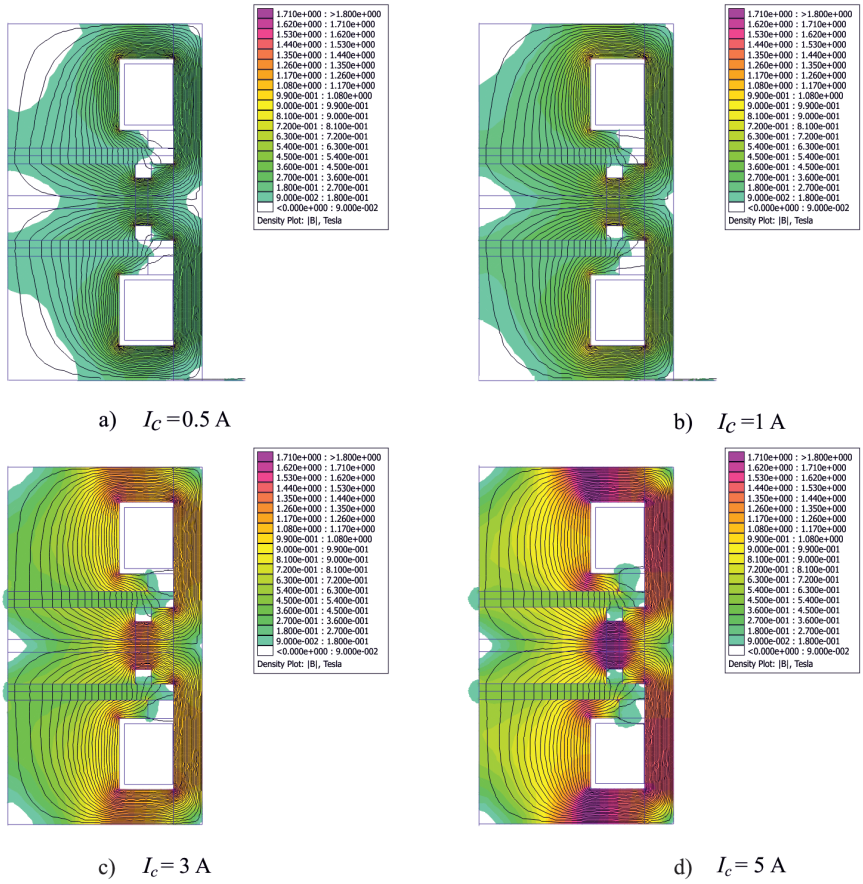

a) $I_C = 0.5$ A b) $I_C = 1$ A

c) $I_c = 3$ A d) $I_c = 5$ A

Fig. 4. Flux density distribution at mid-stroke position of the piston

and Fig. 5b reveals the plot of averaged flux density in the working gap at two positions of the piston (mid-stroke, gap minimum height). Note that this two-coil configuration can be easily adapted to operate in parallel, i.e. the two coils can be controlled independently of each other. It can be shown that, with such an arrangement, the magnetic fluxes generated with the respective coils do not interfere with each other.

Next, flux linkage calculations with respect to current and position change are shown in Fig. 5c. Additionally, coil inductance is computed using the energy method available in the FEMM tool [17]:

$$L_c = \frac{1}{2}\int B \cdot H dV \tag{1}$$

where the integral is obtained over the entire model domain V and L_c denotes the total inductance of the coil. The result is revealed in Fig. 5d. As shown, all static calculations reveal strong dependence on the coil inductance, flux density and flux linkage with respect to both position and current.

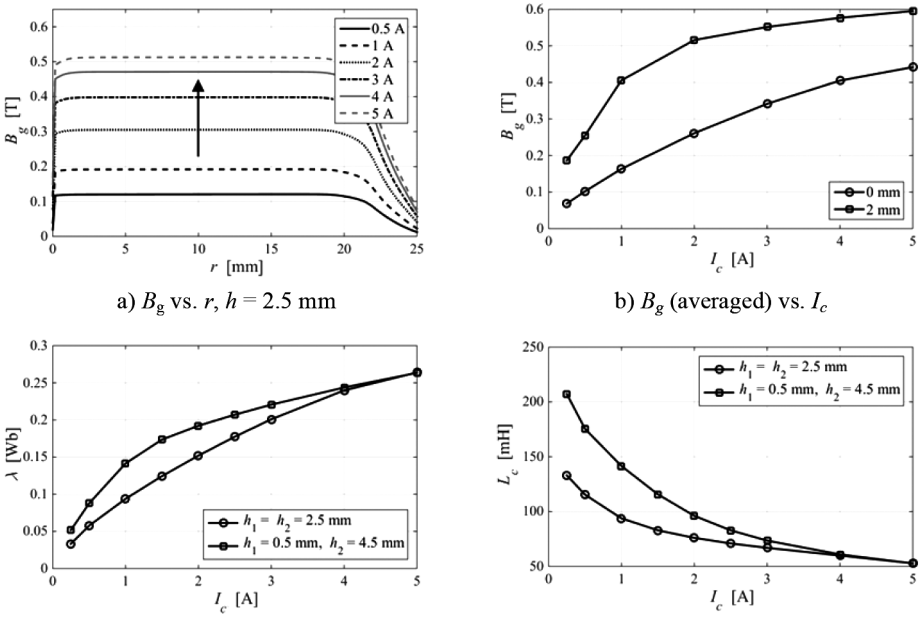

a) B_g vs. r, h = 2.5 mm

b) B_g (averaged) vs. I_c

c) λ vs. I_c

d) L_c vs. I_c

Fig. 5. Magnetostatic analysis results

4. Lumped parameter modeling of the control circuit

In this section, the lumped parameter model of the control circuit, as shown in Fig. 6 has been considered. In the analysis, the model is then coupled with the modified Bingham-Stefan model of the material to provide a multidisciplinary model of the actuator [10, 12].

Moreover, based on the results of the previous section, the authors assumed the flux linkage λ depends on the piston position x and the coil current i_c.

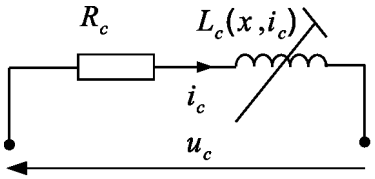

Fig. 6. Lumped parameter circuit of the control coil [18]

Then, the voltage across the coil terminals is:

$$u_c = i_c R_c + \frac{d\lambda}{dt} \tag{2}$$

where R_c is the coil resistance. Therefore, Equation (1) can be expanded to obtain:

$$u_c = i_c R_c + \frac{\partial \lambda}{\partial i_c}\frac{d i_c}{dt} + \frac{\partial \lambda(x, i_c)}{\partial x}\frac{dx}{dt} \tag{3}$$

In order to assess the dynamics of the control, the circuit numerical calculations were carried out using the model given by Equation (2). The results are highlighted in Fig. 7. First, the model was subjected to ramp displacement inputs and step voltage inputs. For instance, Fig. 7a shows the control circuit response as the step voltage was switched ON, and Fig. 7b illustrates the circuit's response during voltage drop (current decay). The results shown in Fig. 7 were obtained by stroking the piston downwards from the mid-stroke at the constant velocity of 2 mm/s. The response time of the coil (defined as the time required to reach 63% of the peak current value) varies from 47 ms (1 A) to 37 ms (5 A). Moreover, the actuator's model was subjected to sinusoidal displacement waveforms of the peak amplitude $X = 2$ mm and frequencies of up to $f = 30$ Hz. Predictably, due to the presence of the velocity–dependent term in Equation (2), the time history of coil current reveals small, yet finite oscillations around the average value of 1 A – see Fig. 8. The data were obtained by exciting the coil with the constant voltage input and cycling the piston according to the prescribed piston displacement $x(t) = h - X\sin(2\pi ft + \varphi)$, where φ is the phase shift. It is evident that the current profile is influenced by both the frequency and the amplitude.

It is also apparent, from the observation of Fig. 8 in particular, that the motional term is not significant (contribution of less than 2% under most circumstances) and can be omitted in further investigations.

In order to study the variation of force output with piston displacement (velocity) and the current applied, the expressions obtained, e.g. by Zhang et al. [10], were used in developing the hydraulic model of the actuator. The expressions utilize the Stefan squeeze-flow solution and were extended to include the two-way action of the piston. The model that was employed by the authors includes the effects of plasticity (due to yield stress), viscous forces and neglects the inertia effects (due to acceleration). By further neglecting the eddy

current effects, coupling the electrical part and the hydraulic component can be directly accomplished through the rheological characteristics of the material, and specifically the $\tau(B = Bg)$ relationship – see Fig. 3b. The simulation results involving the coupled model of the actuator are revealed in Figs. 9 and 10. In the specific examples shown, the piston was subjected to sinusoidal displacement inputs of the peak-to-peak amplitude equal to 4 mm and a frequency of 1 Hz – see Fig 9. The displacement range was designed in such a way to preserve the minimum 0.5 mm gap on either side of the piston.

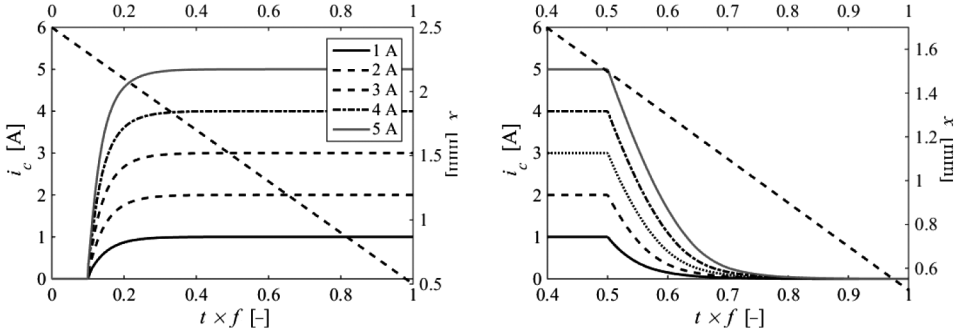

Fig. 7. Coil current response to step voltage input, ramp displacement input: –2 mm/s, $f = 1$ Hz

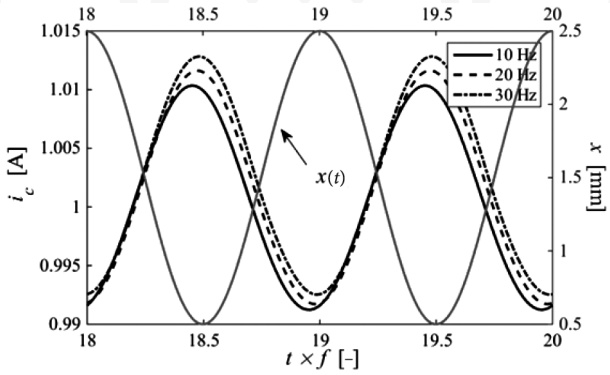

Fig. 8. Time history of coil current: constant voltage, sinusoidal cycling $X = 1$ mm, coil current: 1 A

The displacement range illustrated in Fig. 9 is centered with respect to the middle position of the piston. Throughout the simulation of the results shown in Fig. 9, the supply voltage was held at a fixed level corresponding to the current range from 1 A to 5 A in 1 A intervals. It can be clearly seen that the largest variation of force output occurs in the first and the third quadrants of the force-displacement plane. Moreover, observation of the plot further confirms that the onset of magnetic saturation occurs already at a current level equal to 3 A. Furthermore, the transient response of the actuator was examined while subjecting the piston to ramp displacement (constant velocity) inputs as shown in Fig. 10. While moving

the piston, the current was applied and the resulting response calculated as shown in Fig. 9a. For comparison, in the example shown in Fig. 9b, the current was switched off. By far, the force variation is largest in the case shown in Fig. 9a – the force output is proportional to the inverse of the gap height and is additionally augmented by the field-induced yield stress of the material.

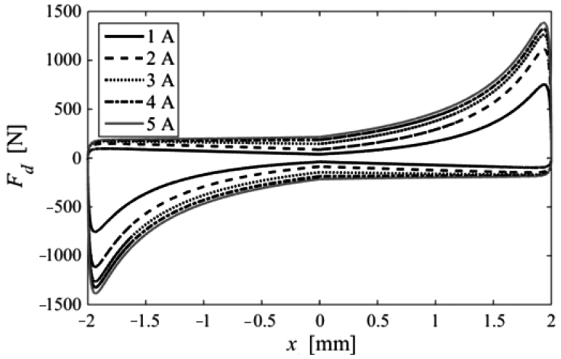

Fig. 9. Force vs displacement loops; sinewave input – $X = 2$ mm, $f = 1$ Hz

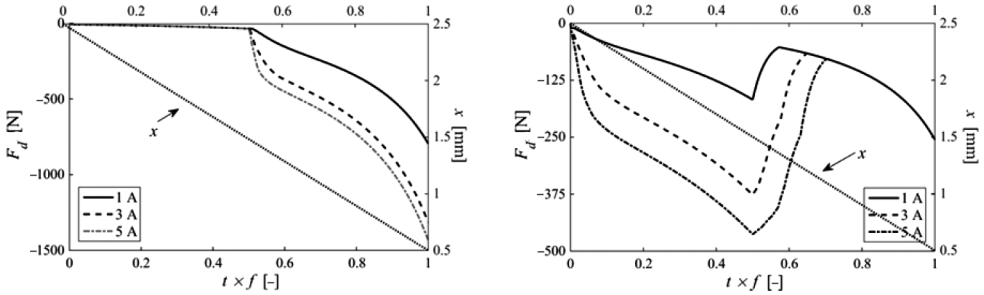

a) OFF-ON b) ON-OFF

Fig. 10. Damping force time history ramp displacement input: 2 mm/s

5. Conclusions

In this paper, the authors reveal the results of a study concerning a two-way MR damper operating in squeeze mode. The device is superior to other concepts of a squeeze-mode damper, as it allows for the realization of vibration control strategies in either direction of the piston motion and for the generation of a symmetric force, both in compression (squeeze) and extension. The authors briefly present magnetic field simulation results in order to assess the device's steady-state performance range. The finite-element analysis is then followed by the study of the coupled (electro-hydraulic) control circuit behavior when subjected to voltage step and displacement inputs. The response of the damper, when subjected to sinusoidal displacement inputs and ramp inputs, was examined, too. The results have indicated that

both the piston position and the current have a significant influence on the damping force output as well as electro-magnetic characteristics of the device incl. flux linkage, coil inductance, averaged flux density. Specifically, flux density, coil inductance and flux linkage vary with both position and current. Finally, it was shown the flux linkage motional term has a little influence on the output of the actuator and could be neglected in further analyses.

References

[1] Rabinov J., *The magnetic field clutch*, AIEE Transactions, vol. 67, 1948, 1308–1315.

[2] Jolly M.R., Bender J.W., Carlson J.D., *Properties and applications of magnetorheological fluids*, Proceedings of the SPIE Conference of the International Society of Optical Engineers (Ed. L. P. Davis), Washington, vol. 3327, 1998, 262–275.

[3] Boelter R., Janocha H., *Performance of long-stroke and low-stroke MR fluid dampers*, Proccedings of the 5th Annual International Symposium on Smart Structures and Materials, 1998, 303–313.

[4] Goncalves F.D., Carlson J.D., *An alternate operation mode for MR fluids – magnetic gradient pinch*, Journal of Physics: Conference Series, vol. 149(1), 2009, 012050.

[5] Alexandridis A., *MagneRide: Magnetorheological fluid-based semi-active suspension*, Proceedings of the European Conference on Vehicle Electronic Systems 2000, Stratford upon Avon (UK), 2000.

[6] Baudendistel T.A., Tewani S.G., Shores J.M., Long M.W., Longhouse R.E., Namuduri C.S., Alexandridis A.A., *Hydraulic mount with magnetorheological fluid*, US Patent No. 6,622,995, 2003.

[7] Barber D.E., Carlson J.D., *Performance characteristics of prototype MR engine mounts containing LORD glycol MR mounts*, Journal of Physics: Conference Series, vol. 149, 2009, 012035.

[8] Carlson J.D., Catanzarite D.M., St. Clair K.M., *Commercial magneto-rheological fluid devices*, International Journal of Modern Physics B, vol. 10.23n24, 1996, 2857–2865.

[9] Carlson J.D*., Multi-degree of freedom magnetorheological devices and system for using same*, U.S. Patent No. 5,492,312. Pub. 20 Feb. 1996.

[10] Zhang X., Farjoud A., Ahmadian M., Guo K., Craft M., *Dynamic testing and modeling of an MR squeeze mount*, Journal of Intelligent Material Systems and Structures, vol. 22(15), 2011, 1717–1728.

[11] Sapiński B., Gołdasz J., *Development and performance evaluation of an MR squeeze-mode damper*, Smart Materials and Structures, vol. 24(11), 2015, 115007.

[12] Gołdasz J., Sapiński B., *Application Of CFD To Modeling Of Squeeze Mode Magnetorheological Dampers*, Acta Mechanica et Automatica, vol. 9(3), 2015, 129–134.

[13] Vieira S. L., Ciocanel C., Kulkami P., Agraval A., Naganathan N., *Behaviour of MR fluids in squeeze mode*, International Journal of Vehicle Design, vol. 33(1–3), 2003, 36–49.

[14] Ruiz-Lopez J. A., Hidalgo-Alvarez R., de Vicente J., *A micromechanical model for magnetorheological fluids under slow compression*, Rheologica Acta, 2015, 10.1007/s00397-016-0910-2.

[15] Gong X., Ruan X., Xuan S., Yan Q., Deng, H., *Magnetorheological Damper Working in Squeeze Mode*, Advances in Mechanical Engineering, vol. 6, 2014, 410158.
[16] Stanway R., Sims N. D., Johnson A. R., *Modeling and control of a magnetorheological vibration isolator*, Proceedings of the SPIE's 7th Annual International Symposium on Smart Structures and Materials, Newport Beach, CA, vol. 3989, 2000, 184–193.
[17] Meeker D., *Finite Element Method Magnetics. Version 4.2. User's Manual*, 2006.
[18] Sapiński B., Krupa S., Matras A., *Symulacja obwodu sterującego tłumika z cieczą MR działającą w trybie ściskania*, Przegląd Elektrotechniczny, vol. 91(8), 2015, 135–138.
[19] Farjoud A., *Magneto-rheological fluid behavior in squeeze mode*, Smart Materials and Structures, vol. 18(9), 2009, 095001.
[20] Farjoud A., et al., *Experimental investigation of MR squeeze mounts*, Journal of Intelligent Material Systems and Structures, vol. 22(15), 2011, 1645–1652.
[21] Kieburg Ch., *MR Fluid Basonetic 4035*, BASF Technical Information, 2010.